NANO LETTERS

pubs.acs.org/NanoLett
Letter

Stress-Dependent Optical Extinction in Low-Pressure Chemical Vapor Deposition Silicon Nitride Measured by Nanomechanical Photothermal Sensing

Kostas Kanellopulos, Robert G. West, Stefan Emminger, Paolo Martini, Markus Sauer, Annette Foelske, and Silvan Schmid*

Cite This: *Nano Lett.* 2024, 24, 11262−11268

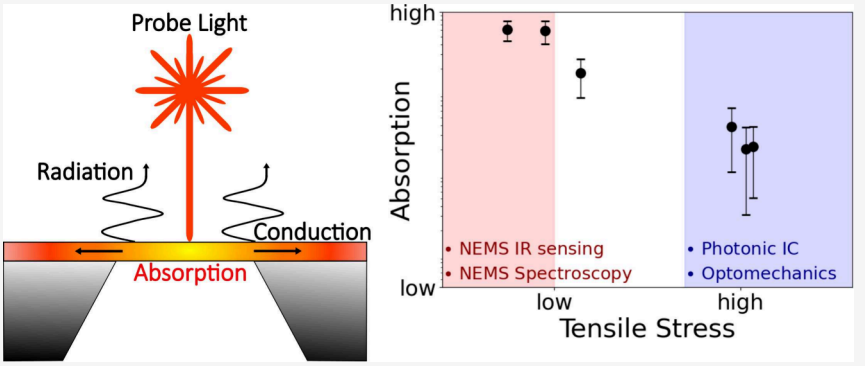

ABSTRACT: Understanding optical absorption in silicon nitride is crucial for cutting-edge technologies like photonic integrated circuits, nanomechanical photothermal infrared sensing and spectroscopy, and cavity optomechanics. Yet, the origin of its strong dependence on the film deposition and fabrication process is not fully understood. This Letter leverages nanomechanical photothermal sensing to investigate optical extinction κ_{ext} at a 632.8 nm wavelength in low-pressure chemical vapor deposition (LPCVD) SiN strings across a wide range of deposition-related tensile stresses (200−850 MPa). Measurements reveal a reduction in κ_{ext} from 10^3 to 10^1 ppm with increasing stress, correlated to variations in Si/N content ratio. Within the band-fluctuations framework, this trend indicates an increase of the energy bandgap with the stress, ultimately reducing absorption. Overall, this study showcases the power and simplicity of nanomechanical photothermal sensing for low absorption measurements, offering a sensitive, scattering-free platform for material analysis in nanophotonics and nanomechanics.

KEYWORDS: *absorption, extinction, nanomechanics, nanophotonics, optics, photonics*

Investigating the optical properties of solid-state materials is essential for both fundamental and applied science. Optical absorption, in particular, is critical in various fields, including photonic integrated circuits (PIC) for quantum information,[1] and the design of nanomechanical resonant sensors for infrared (IR) light detection,[2] photothermal spectromicroscopy,[3−5] and cavity optomechanics.[6−10]

In IR sensing, high optical absorption is desired to enhance the sensor's specific detectivity.[2,11] Conversely, applications like PICs, cavity optomechanics, and nanomechanical photothermal spectromicroscopy require minimal absorption to realize high-confinement waveguides,[12] to prevent mechanical instability[10,13] and cavity bistability,[14] and to mitigate photothermal back-action frequency noise introduced in the resonator,[15] respectively.

Silicon nitride (SiN) holds a prominent position in these fields for its excellent mechanical, thermal, and optical properties.[16,17] Its extensive use in photonics stems from its broad transparency window (0.4−8 μm), which, however, strongly depends on the film deposition and fabrication process, for which the underlying mechanisms are not fully understood. This has been observed by means of various characterization techniques, such as ellipsometry,[18−23] direct single-pass absorption spectroscopy,[24] FTIR interferometry,[25,26] cutback,[27] outscattered light method,[28−32] prism coupling,[33] photoluminescence,[34] photothermal common-path interferometry,[35] and cavity-enhanced absorption spectroscopy.[12,16,36] However, these approaches often suffer from

Received: June 19, 2024
Revised: August 22, 2024
Accepted: August 23, 2024
Published: August 30, 2024

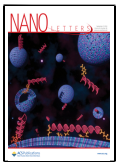

https://doi.org/10.1021/acs.nanolett.4c02902
Nano Lett. 2024, 24, 11262−11268

scattering losses and slow measurement time, which obscure the true absorption of SiN and make analyses prone to parasitic heating of the surroundings.

Within this context, nanomechanical photothermal spectroscopy offers a robust solution to these challenges.[4,37−42] Here, a tensile stressed nanomechanical resonator detects directly absorption via resonance frequency shifts due to photothermal heating, insensitive to scattering. Upon illumination, the resultant temperature rise makes the initial tensile stress relax, leading to frequency detuning. Due to its high power sensitivity, fast thermal response, and versatility in sensor design, this technique has significantly advanced the characterization of low-loss materials.[5]

In this Letter, nanomechanical photothermal sensing is employed to elucidate the relationship between absorption and residual tensile stress in low-pressure chemical vapor deposition (LPCVD) deposited SiN thin films. The extinction coefficient at 632.8 nm wavelength is measured from low stress (≈200 MPa), relevant to photothermal-based applications,[5] to high stress (>800 MPa), relevant to cavity optomechanics[43,44] and PIC design.[12] The thin films are patterned in a string geometry, which ensures high photothermal responsivity and fast response, as previously demonstrated.[15] The experimental results reveal a reduction in extinction (from 10^3 to 10^1 ppm) with increasingly higher tensile stress, consistent with previously observed trends.[23] The measurements are analyzed within the framework of the band-fluctuations model,[45] attributing the observed reduction to a blue-shift in the energy bandgap caused by a decrease in silicon-to-nitrogen (Si/N) content ratio. Overall, this study underscores the power and simplicity of nanomechanical photothermal sensing for the characterization of low-loss materials in nanophotonics and nanomechanics.

In the present setup, the nanomechanical resonator is operated in a custom-made vacuum chamber at high-vacuum conditions ($p < 10^{-5}$ mbar) to reduce gas damping and thermal convection losses.[4] The mechanical displacement is transduced optically via laser-Doppler vibrometry (LDV, Polytec GmbH MSA-500) equipped with a HeNe laser at 632.8 nm wavelength, with a beam waist of ≈1.5 μ m (Figure 1). The same laser also probes SiN absorption, which simplifies the measurement procedure. For each structure, the frequency shift of the thermomechanical noise peak for the fundamental resonance mode is recorded at various optical powers (6−120 μW),[15,46] as schematically shown in Figure 1b. Here, the plot shows the displacement power spectral density (PSD), in units [m^2/Hz], around the fundamental mechanical resonance. Its peak $S_{zz,thm}$, well resolved by the vibrometer ($S_{zz,thm} \gg S_{det}$, with S_{det} denoting the detection noise PSD), red-shifts as the impinging optical power increases ($f_i > f_{i+1}$ for $P_i < P_{i+1}$). For each experimental result, the system has been measured in the steady state, recording the signal for a measurement time $\tau_{meas} > \tau_{th}$, with τ_{th} denoting the time required for the resonator to reach this steady state (see eq 1).[15] A minimum of five resonators is evaluated for each stress and length, with fundamental resonance frequencies ranging from 60 kHz (for L = 2 mm and σ_0 = 174 MPa) to 2.6 MHz (for L = 0.1 mm and σ_0 = 835 MPa). Figure 1c shows a representative image of the characterized strings.

The absorption coefficient α_{abs} is determined via comparison between the theoretical $\mathcal{R}_P$ and the experimental $\mathcal{R}_{P_0}$ relative power responsivity for the string resonators.[5,15,47] On the one hand, $\mathcal{R}_P$ denotes the relative frequency change per absorbed power $P(\lambda) = \alpha_{abs}(\lambda)P_0$ and is expressed as[47]

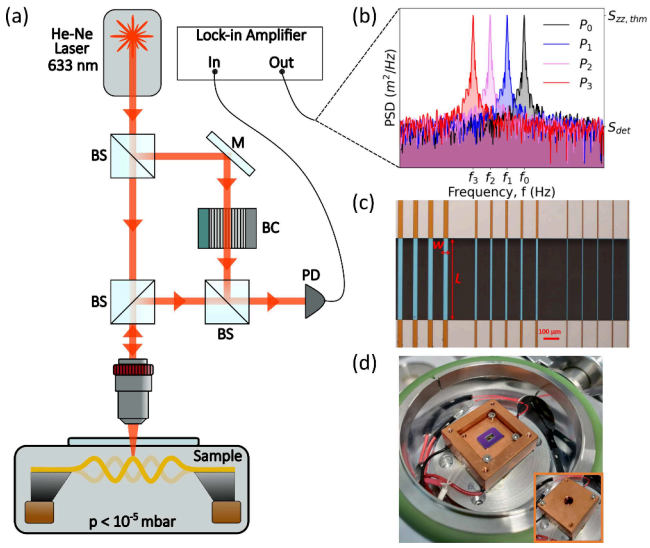

Figure 1. (a) Sketch of the experimental setup (LDV MSA-500, Polytech GmbH). A laser of wavelength λ and input power P_0 impinges on the resonator, of absorption coefficient $\alpha_{abs}(\lambda)$. This causes a frequency detuning of the nanomechanical resonator. BS: beam splitter. BC: Bragg cell. PD: photodetector. (b) Mechanical frequency detuning measured by monitoring the shift of the thermomechanical noise peak of the string's fundamental mode as a function of P_0. The peak $S_{zz,thm}$ is given in terms of displacement power spectral density (PSD) [m^2/Hz] and is well resolved by the vibrometer ($S_{zz,thm} \gg S_{det}$, with S_{det} denoting the detection noise PSD). In the x-axis, $f_i = f_{res}(P_i)$, with i = 1, 2, ⋯, is the resonance frequency of the fundamental mode at each input laser power $P_i > P_{i-1}$. (c) Optical micrograph of the SiN strings used in the present study. Orange/light blue regions are made of SiN; the gray regions are the Si substrate. (d) Photo of the cm-scale copper thermal equilibrium chamber used for the characterization of the linear coefficient of thermal expansion. A thermoelectric module is glued beneath to heat the whole oven (thick red electrical connections) to guarantee a uniform temperature rise of the chips. The temperature is monitored and kept constant with a PID controller.

$$\mathcal{R}_P(\omega) = \frac{1}{f_0}\frac{\partial f_0}{\partial P} = \frac{\mathcal{R}_T}{G}|H_{th}(\omega)| \tag{1}$$

where $\mathcal{R}_T$, G, and $H_{th}(\omega) = (1 + i\omega\tau_{th})^{-1}$ denote the temperature responsivity in units [1/K], the thermal conductance in units [W/K], and the thermal response of the resonator, with τ_{th} its thermal time constant, respectively.[15,47] As already mentioned, all the measurements have been performed far from any thermal transient ($\omega \ll \tau_{th}^{-1}$), i.e., in the steady-state. Hence, the ω-dependence is dropped in the following.

For a string resonator, eq 1 is given by[47]

$$\mathcal{R}_P = -\frac{\alpha_{th}E}{2\sigma_0}\left[8\frac{hw}{L}\kappa + 8Lw\epsilon_{rad}\sigma_{SB}T_0^3\right]^{-1} \tag{2}$$

with α_{th}, E, σ_0, h, w, L, κ, ϵ_{rad}, σ_{SB}, and T_0 denoting the resonator's linear coefficient of thermal expansion, Young's modulus, tensile stress, thickness, width, length, thermal conductivity, emissivity, Stefan−Boltzmann constant, and bath temperature, respectively. The thermal conductance G includes the thermal dissipation through the surrounding

https://doi.org/10.1021/acs.nanolett.4c02902
Nano Lett. 2024, 24, 11262−11268

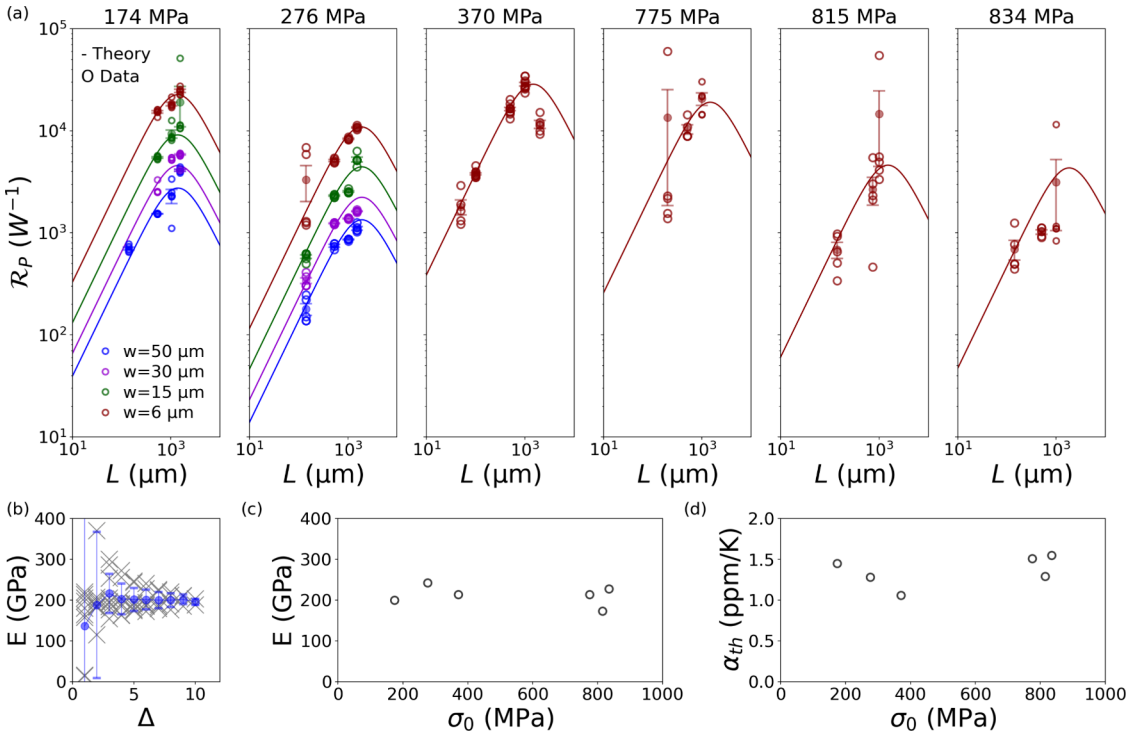

Figure 2. (a) $\mathcal{R}_P$ for different SiN string structures. Circles: experimental responsivity (3), divided by the corresponding mean absorption coefficient α_{abs}. Solid curve: theoretical model (2). Material parameter assumed: ρ = 3000 kg/m^3, κ = 3 W/(m K). Emissivity values are calculated from data reported in ref 25: 0.05 (h = 56 nm), 0.13 (h = 157 nm), 0.133 (h = 177 nm), 0.171 (h = 312 nm), 0.176 (h = 340 nm). (b) Example of Young's modulus estimation, following the procedure of ref 48. (c) Experimental Young's modulus E as a function of the prestress σ_0. (d) Experimental linear coefficient of thermal expansion α_{th} as a function of the prestress σ_0.

Table 1. String Resonators' Geometrical (h), Mechanical (σ_0, E, α_{th}), Compositional (Si/N), and Optical (η, κ_{ext}, E_g, β^{-1}) Properties

σ_0 (MPa)	h (nm)	E (GPa)	α_{th} (ppm/K)	η	κ_{ext} (ppm)	Si/N	E_g (eV)	β^{-1} (meV)
174	177	200	1.45	1.215	606	0.96	3.23	201
275	340	243	1.28	1.105	588	0.98	3.09	183
370	56	214	1.06	1.022	176	0.89	3.62	212
775	56	214	1.51	1.022	38	0.86	3.90	208
815	157	173	1.29	1.273	20	0.83	4.21	227
834	312	227	1.55	1.268	21	0.84	4.10	217

frame G_{cond} (first addend in brackets) and thermal radiation to the environment G_{rad} (second addend in brackets).[15,47]

$\mathcal{R}_{P_0}$ is obtained by directly measuring the relative frequency shift per impinging power P_0 (as schematically shown in Figure 1b). It relates to $\mathcal{R}_P$ through the absorption coefficient $\alpha_{abs}(\lambda)$ as follows

$$\mathcal{R}_{P_0}(\lambda) = \frac{1}{f_0}\frac{\partial f_0}{\partial P_0} = \frac{1}{f_0}\frac{\partial f_0}{\partial P}\frac{\partial P}{\partial P_0} = \alpha_{abs}(\lambda)\mathcal{R}_P \tag{3}$$

with λ denoting the probe optical wavelength. From eq 3, it is possible to directly evaluate the optical absorption coefficient as $\alpha_{abs} = \mathcal{R}_{P_0}/\mathcal{R}_P$.

The experimental power responsivity (3) across the different stresses is displayed in Figure 2a as a function of the resonators' length L (circles), together with the theoretical calculations (2) (solid curves). The scale is given in terms of absorbed power P. It is worth noting that $\mathcal{R}_P$ grows for longer strings in the conduction-limited regime (L < 1 mm), as $G \simeq G_{cond}$ is inversely proportional to the length L (see eq 2), leading to better thermal insulation from the environment.[15] Conversely, increasingly longer resonators (L > 1 mm) enter the radiation-limited regime ($G \simeq G_{rad}$), leading to a drop of $\mathcal{R}_P$ as the radiating surface increases.

The analyzed resonators have thicknesses of h = 56−340 nm and widths of w = 5−50 μm, ensuring minimal thermal dissipation. As indicated in eq 2, $G_{cond} \propto hw$ and $G_{rad} \propto w$, making these strings highly responsive to photothermal heating. Furthermore, the length L varies in the range 0.1−2 mm, making the resonator's power response mainly thermal conduction limited.[15] The current experimental approach is, therefore, less influenced by the SiN emissivity, which, according to Kirchhoff's law, equals the optical absorption[49]—the parameter under scrutiny in this study. Moreover, the temperature responsivity $\mathcal{R}_T$ appearing in eq 2 is independent of the Poisson's ratio ν, opposite to what occurs in, e.g., membrane resonators,[15,47] which further reduces the uncertainty in the absorption measurement stemming from its dependence on other material parameters. Hence, the resonators employed here make this approach highly robust for solid-state material absorption characterization.

https://doi.org/10.1021/acs.nanolett.4c02902
Nano Lett. 2024, 24, 11262−11268

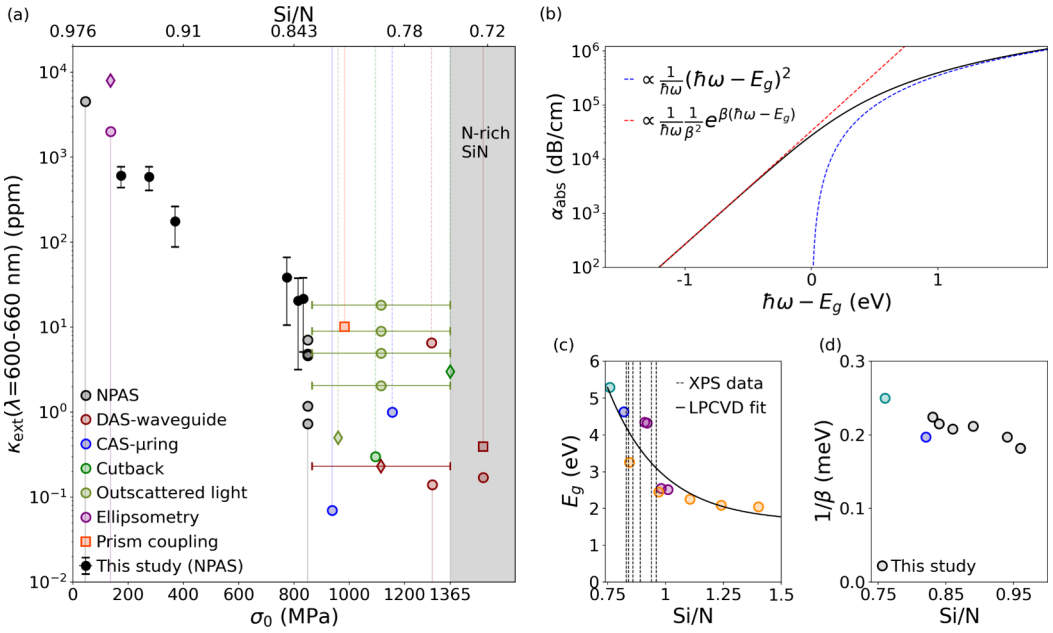

Figure 3. (a) κ_{ext} for different SiN string's tensile stresses at an excitation wavelength of λ = (632.8 ± 30) nm. Characterization techniques included in the figure are: nanomechanical photothermal absorption spectroscopy (NPAS),[42] direct absorption spectroscopy (DAS) in waveguides,[52−55] cavity absorption spectroscopy in microring resonators (CAS-μring),[12,56] cutback,[27] ellipsometry,[19] and prism coupling.[33] Markers refer to LPCVD (circles), plasma-enhanced CVD (PECVD, diamonds), and electron-cyclotron resonance CVD (ECR-CVD, squares) deposited SiN films. For the reported values, the vertical lines indicate a relationship with stress σ_0 (intersection with the bottom x-axis) or Si/N (intersection with the top x-axis), explicitly given in (solid lines) or derived from (dashed lines) the original article. When none of these values could be extracted, a stress error bar has been used (σ_0 = 865−1365 MPa). (b) Absorption coefficient in the band-fluctuations model. The dashed blue and red curves represent the absorption due to electronic transition between extended states (Tauc regime) and absorption due to disorder-induced localized to extended state transitions (Urbach regime), respectively. (c) Energy bandgap E_g as a function of the Si/N ratio. The solid curve is a fitting function of the displayed reported values of the form $f(x) = ae^{-bx} + c$, with a = 95.94 eV, b = 4.356, and c = 1.633 eV. Only LPCDV SiN films have been considered. Compilation: dark cyan, ref 57; blue, ref 12; purple, ref 23; orange, ref 21. Dashed vertical lines indicate the Si/N ratios measured in this study with XPS. Intersections with the fitting curve are given in Table 1. (d) Corresponding Urbach energy β^{-1} of the thin films analyzed in this study (black circles). For comparison, data from ref 57 (dark cyan) and ref 12 (blues) are displayed.

In this regard, the Young's modulus E and the linear coefficient of thermal expansion α_{th} have been measured to reduce the uncertainty on the estimation of the absorption coefficient α_{abs}. E has been estimated following the procedure of ref 48, upon recording of the strings' eigenmode spectrum (an example is displayed in Figure 2b, where $\Delta = |m - n|$, with $n \neq m$ being modal numbers). The experimental results are displayed in Figure 2c and Table 1, with values in the range 170−250 GPa, consistent with previously reported data.[17,48]

α_{th} has been measured by recording the frequency shift of the thermomechanical noise peak as a function of controlled temperature rises (ΔT = 0−10 K),[50] through the relation $\alpha_{th,SiN} = \alpha_{th,Si} - 2\mathcal{R}_T\sigma_0/E$. For that, a thermoelectric module (GM200−127−10−15, Adaptive Power Management) has been used to heat up the resonators, while monitoring and keeping the temperature at the desired value via a PID controller (TEC-1092, Meerstetter Engineering). The chips have been enclosed inside a cm-scale copper thermal bath to guarantee thermal equilibrium through radiative heat transfer of the string with the environment (see Figure 1d). Figure 2d and Table 1 show the corresponding results, with α_{th} lying in the range 1−1.6 ppm/K (assuming $\alpha_{th,Si}$ = 2.6 ppm/K), which are consistent with previously reported values.[17,50] No stress dependence has been observed for the two material parameters.

From the absorption measurements, the extinction coefficient for these thin films can be evaluated as[51]

$$\kappa_{ext}(\lambda) = \frac{\lambda\alpha_{abs}(\lambda)}{4\pi h\eta} \tag{4}$$

with η denoting a dimensionless factor that accounts for possible interference inside the thin SiN slab.[42] For the film thicknesses analyzed here, $\eta \approx 1-1.27$ at 632.8 nm wavelength (see Table 1 and Supporting Information). Figure 3a shows the nanomechanical photothermal results of κ_{ext} as a function of the resonators' tensile stress σ_0 (black circles). κ_{ext} decreases from $\approx 10^3$ ppm for the lowest stress to $\approx 10^1$ ppm for the highest. These findings are compared with previously reported values of optical extinction for LPCVD (colored circles), as well as PECVD (colored diamonds), and ECR-CVD (colored squares) deposited SiN films (see Supporting Information for details on their deposition dependencies). The variance in magnitude among the compiled data for $\sigma_0 \geq 850$ MPa can be partially attributed also to the inability of some of the considered techniques to differentiate between true absorption and scattering losses (in particular cutback and outscattered light[12]). Overall, a general trend emerges in Figure 3a, with κ_{ext} decreasing for increasingly higher SiN deposition-related tensile stress.

The measurements are analyzed within the framework of the band-fluctuations model,[45] which describes the absorption coefficient in units of [dB/m] as a function of the excitation energy $\hbar\omega$ for amorphous materials as

https://doi.org/10.1021/acs.nanolett.4c02902
Nano Lett. 2024, 24, 11262−11268

$$\alpha_{abs}(\hbar\omega) = \frac{\alpha_0}{\hbar\omega}\frac{1}{\beta^2}\mathcal{J}_{cv}(\beta(\hbar\omega - E_g)) \quad (5)$$

where α_0, β, E_g, and $\mathcal{J}_{cv}$ denote a coefficient collecting physical constants in unit $[(\mathrm{m\ eV})^{-1}]$, the Urbach slope in units $[\mathrm{eV}^{-1}]$, the energy bandgap in units [eV], and a dimensionless joint electronic density of states (DOS), respectively. Figure 3b displays its functional form. For excitation energies $\hbar\omega > E_g$, eq 5 converges to the Tauc regime,[23] where only fundamental electronic transitions between extended states are considered (dashed blue curve); for $\hbar\omega < E_g$, the model converges to the empirical Urbach tail, where electronic defect-induced absorption follows $\alpha_{abs} \propto e^{\beta\hbar\omega}$ (dashed red curve).[45]

The model input parameters E_g and the Urbach energy β^{-1} depend on the film deposition process through the residual tensile stress present in the films. In turn, this dependence is underpinned by the underlying correlation between the stress and the corresponding Si/N ratio, with the former increasing as the latter is reduced (see Table 1), as observed in LPCVD, as well as PECVD and ECR-CVD deposited SiN films.[21,23,58] Hence, the optical extinction reduction observed in Figure 3a for increasing tensile stress has to be related to the difference in the chemical composition of the thin films.

In this regard, the Si/N ratio of each chip has been experimentally characterized by X-ray photoelectron spectroscopy (XPS, PHI Versa Probe III-spectrometer) equipped with a monochromatic Al-K_α X-ray source and a hemispherical analyzer. Data analysis was performed using CASA XPS and Multipak software packages (see Supporting Information for more details). The results are displayed in Table 1 and are consistent with those reported in previous works for similar tensile stress range.[23,26,58] These values are also shown in the top x-axis of Figure 3a, to highlight how SiN extinction increases with Si/N.

Finally, the energy bandgap E_g of each thin film has been extracted by means of the fitting curve constructed from the compilation of previous works on LPCVD SiN only,[12,21,23,57] which are shown in Figure 3c. The XPS data (dashed vertical lines) are shown for clarity, and fall in the region of strongest dependence on Si/N. The corresponding energy bandgap (Table 1) has been found to increase from ≈3 eV, for the highest relative Si concentration, to ≈4.2 eV, for the lowest. All these values exceed the probing energy used in this study ($\hbar\omega$ = 1.96 eV), indicating that the absorption results from localized-to-extended electronic transitions of disorder-induced tail states, as it occurs typically in amorphous semiconductors.[45]

With the energy bandgap defined for each thin film, the corresponding Urbach energy β^{-1} has been determined by matching the experimental absorption to the band-fluctuations model. The results are shown in Figure 3d and Table 1, and are consistent with previously reported studies of LPCVD SiN ($\beta^{-1} \approx 200$ meV).[12,57] β^{-1} slightly decreases with increasing Si/N ratios, as it has been observed also for PECVD deposited SiN, but at lower values (see the Supporting Information for a comparison).[59,60] Hence, lowering the Si/N ratio has the main effect of shifting the bandgap E_g to higher energies, broadening the SiN transparency window. Conversely, the Urbach energy β^{-1} does not vary significantly among these thin films, indicating that the reduction in extinction coefficient κ_{ext} is driven by an exponential decrease in the disorder-induced electronic tail DOS at the probing energy of 1.96 eV.

In conclusion, it has been shown that nanomechanical photothermal spectroscopy represents a highly sensitive, simple, and scattering-free platform for the optical characterization of low-loss materials. In this study, its capabilities have been explored using nanostring resonators made of LPCVD deposited SiN. Upon meticulous characterization of their mechanical and thermomechanical properties, it has been shown that SiN intrinsic extinction coefficient decreases with increasingly higher thin film tensile stress. This trend is attributed to a blue-shift in energy bandgap as a function of material composition. Therefore, varying the Si/N ratio provides a degree of freedom to tune the optical properties of SiN, advancing the understanding of this ubiquitous material.

■ ASSOCIATED CONTENT

Supporting Information

The Supporting Information is available free of charge at https://pubs.acs.org/doi/10.1021/acs.nanolett.4c02902

Calculation of the emissivity and factor η for different thicknesses; compilation of data (table); derivation of Si/N ratios for the compiled data; comparison of the measured Urbach energies with reported data for LPCVD and PECVD SiN films; and details on the XPS measurements (PDF)

■ AUTHOR INFORMATION

Corresponding Author

Silvan Schmid − *Institute of Sensor and Actuator Systems, TU Wien, 1040 Vienna, Austria;* orcid.org/0000-0003-3778-7137; Email: silvan.schmid@tuwien.ac.at

Authors

Kostas Kanellopulos − *Institute of Sensor and Actuator Systems, TU Wien, 1040 Vienna, Austria;* orcid.org/0000-0002-5982-9724

Robert G. West − *Institute of Sensor and Actuator Systems, TU Wien, 1040 Vienna, Austria;* orcid.org/0000-0001-8005-644X

Stefan Emminger − *Institute of Sensor and Actuator Systems, TU Wien, 1040 Vienna, Austria*

Paolo Martini − *Institute of Sensor and Actuator Systems, TU Wien, 1040 Vienna, Austria*

Markus Sauer − *Analytical Instrumentation Center, TU Wien, 1060 Vienna, Austria*

Annette Foelske − *Analytical Instrumentation Center, TU Wien, 1060 Vienna, Austria*

Complete contact information is available at: https://pubs.acs.org/10.1021/acs.nanolett.4c02902

Notes

The authors declare no competing financial interest.

■ ACKNOWLEDGMENTS

The authors thank Johannes Hiesberger for the help with the experimental setup and Hajrudin Besic, Nicola Cavalleri, and Niklas Luhmann for useful discussions. This project received funding from the Novo Nordisk Foundation under project MASMONADE with project number NNF22OC0077964. Moreover, the Austrian Research Promotion Agency (FFG) is gratefully acknowledged for funding of the used XPS infrastructure (FFG project number: 884672).

REFERENCES

(1) Moody, G.; et al. 2022 Roadmap on integrated quantum photonics. *J. Phys. Photonics* **2022**, *4*, No. 012501.
(2) Piller, M.; Hiesberger, J.; Wistrela, E.; Martini, P.; Luhmann, N.; Schmid, S. Thermal IR Detection With Nanoelectromechanical Silicon Nitride Trampoline Resonators. *IEEE Sens. J.* **2023**, *23*, 1066−1071.
(3) Kirchhof, J. N.; Yu, Y.; Yagodkin, D.; Stetzuhn, N.; de Araújo, D. B.; Kanellopulos, K.; Manas-Valero, S.; Coronado, E.; van der Zant, H.; Reich, S.; Schmid, S.; Bolotin, K. I. Nanomechanical absorption spectroscopy of 2D materials with femtowatt sensitivity. *2D Mater.* **2023**, *10*, No. 035012.
(4) Kanellopulos, K.; West, R. G.; Schmid, S. Nanomechanical Photothermal Near Infrared Spectromicroscopy of Individual Nanorods. *ACS Photonics* **2023**, *10*, 3730−3739.
(5) West, R. G.; Kanellopulos, K.; Schmid, S. Photothermal Microscopy and Spectroscopy with Nanomechanical Resonators. *J. Phys. Chem. C* **2023**, *127*, 21915−21929.
(6) Wilson, D. J. Cavity Optomechanics with High-Stress Silicon Nitride Films. *Ph.D. Dissertation*; California Institute of Technology, 2012.
(7) Reinhardt, C.; Müller, T.; Bourassa, A.; Sankey, J. C. Ultralow-Noise SiN Trampoline Resonators for Sensing and Optomechanics. *Phys. Rev. X* **2016**, *6*, No. 021001.
(8) Gärtner, C.; Moura, J. P.; Haaxman, W.; Norte, R. A.; Gröblacher, S. Integrated Optomechanical Arrays of Two High Reflectivity SiN Membranes. *Nano Lett.* **2018**, *18*, 7171−7175.
(9) Mason, D.; Chen, J.; Rossi, M.; Tsaturyan, Y.; Schliesser, A. Continuous force and displacement measurement below the standard quantum limit. *Nat. Phys.* **2019**, *15*, 745−749.
(10) Huang, G.; Beccari, A.; Engelsen, N. J.; Kippenberg, T. J. Room-temperature quantum optomechanics using an ultralow noise cavity. *Nature* **2024**, *626*, 512−516.
(11) Snell, N.; Zhang, C.; Mu, G.; Bouchard, A.; St-Gelais, R. Heat Transport in Silicon Nitride Drum Resonators and its Influence on Thermal Fluctuation-Induced Frequency Noise. *Phys. Rev. Appl.* **2022**, *17*, No. 044019.
(12) Corato-Zanarella, M.; Ji, X.; Mohanty, A.; Lipson, M. Absorption and scattering limits of silicon nitride integrated photonics in the visible spectrum. *Opt. Express* **2024**, *32*, 5718.
(13) Metzger, C.; Ludwig, M.; Neuenhahn, C.; Ortlieb, A.; Favero, I.; Karrai, K.; Marquardt, F. Self-Induced Oscillations in an Optomechanical System Driven by Bolometric Backaction. *Phys. Rev. Lett.* **2008**, *101*, 133903.
(14) An, K.; Sones, B. A.; Fang-Yen, C.; Dasari, R. R.; Feld, M. S. Optical bistability induced by mirror absorption: measurement of absorption coefficients at the sub-ppm level. *Opt. Lett.* **1997**, *22*, 1433.
(15) Kanellopulos, K.; Ladinig, F.; Emminger, S.; Martini, P.; West, R. G.; Schmid, S. Comparative Analysis of Nanomechanical Resonators: Sensitivity, Response Time, and Practical Considerations in Photothermal Sensing. *arXiv* **2024**; https://arxiv.org/abs/2406.03295, [physics.app-ph]. Submitted on June 5, 2024.
(16) Ji, X.; Okawachi, Y.; Gil-Molina, A.; Corato-Zanarella, M.; Roberts, S.; Gaeta, A. L.; Lipson, M. Ultra-Low-Loss Silicon Nitride Photonics Based on Deposited Films Compatible with Foundries. *Laser Photonics Rev.* **2023**, *17*, 2200544.
(17) Kaloyeros, A. E.; Pan, Y.; Goff, J.; Arkles, B. Review—Silicon Nitride and Silicon Nitride-Rich Thin Film Technologies: State-of-the-Art Processing Technologies, Properties, and Applications. *ECS J. Solid State Sci. Technol.* **2020**, *9*, No. 063006.
(18) Makino, T. Composition and Structure Control by Source Gas Ratio in LPCVD SiNx. *J. Electrochem. Soc.* **1983**, *130*, 450.
(19) Poenar, D. P.; Wolffenbuttel, R. F. Optical properties of thin-film silicon-compatible materials. *Appl. Opt.* **1997**, *36*, 5122.
(20) Lin, P. T.; Singh, V.; Lin, H. Y. G.; Tiwald, T.; Kimerling, L. C.; Agarwal, A. M. Low-stress silicon nitride platform for mid-infrared broadband and monolithically integrated microphotonics. *Adv. Opt. Mater.* **2013**, *1*, 732−739.
(21) Krückel, C. J.; Fülöp, A.; Ye, Z.; Andrekson, P. A.; Torres-Company, V. Optical bandgap engineering in nonlinear silicon nitride waveguides. *Opt. Express* **2017**, *25*, 15370.
(22) Resende, J.; Fuard, D.; Le Cunff, D.; Tortai, J.-H.; Pelissier, B. Hybridization of ellipsometry and energy loss spectra from XPS for bandgap and optical constants determination in SiON thin films. *Mater. Chem. Phys.* **2021**, *259*, 124000.
(23) Beliaev, L. Y.; Shkondin, E.; Lavrinenko, A. V.; Takayama, O. Optical, structural and composition properties of silicon nitride films deposited by reactive radio-frequency sputtering, low pressure and plasma-enhanced chemical vapor deposition. *Thin Solid Films* **2022**, *763*, 139568.
(24) Philipp, H. R. Optical Properties of Silicon Nitride. *J. Electrochem. Soc.* **1973**, *120*, 295.
(25) Cataldo, G.; Beall, J. A.; Cho, H.-M.; McAndrew, B.; Niemack, M. D.; Wollack, E. J. Infrared dielectric properties of low-stress silicon nitride. *Opt. Lett.* **2012**, *37*, 4200−4202.
(26) Yang, C.; Pham, J. Characteristic Study of Silicon Nitride Films Deposited by LPCVD and PECVD. *Silicon* **2018**, *10*, 2561−2567.
(27) Sorace-Agaskar, C.; Kharas, D.; Yegnanarayanan, S.; Maxson, R. T.; West, G. N.; Loh, W.; Bramhavar, S.; Ram, R. J.; Chiaverini, J.; Sage, J.; Juodawlkis, P. Versatile Silicon Nitride and Alumina Integrated Photonic Platforms for the Ultraviolet to Short-Wave Infrared. *IEEE J. Sel. Top. Quantum Electron.* **2019**, *25*, 1−15.
(28) Smith, J. A.; Francis, H.; Navickaite, G.; Strain, M. J. SiN foundry platform for high performance visible light integrated photonics. *Opt. Mater. Express* **2023**, *13*, 458.
(29) Blasco-Solvas, M.; Fernández-Vior, B.; Sabek, J.; Fernández-Gavela, A.; Domínguez-Bucio, T.; Gardes, F. Y.; Domínguez-Horna, C.; Faneca, J. Silicon Nitride Building Blocks in the Visible Range of the Spectrum. *J. Light. Technol.* **2024**, *42*, 6019−6027.
(30) Lelit, M.; Słowikowski, M.; Filipiak, M.; Juchniewicz, M.; Stonio, B.; Michalak, B.; Pavłov, K.; Myśliwiec, M.; Wiśniewski, P.; Kaźmierczak, A.; Anders, K.; Stopiński, S.; Beck, R. B.; Piramidowicz, R. Passive Photonic Integrated Circuits Elements Fabricated on a Silicon Nitride Platform. *Materials* **2022**, *15*, 1398.
(31) Mashayekh, A. T.; Klos, T.; Geuzebroek, D.; Klein, E.; Veenstra, T.; Büscher, M.; Merget, F.; Leisching, P.; Witzens, J. Silicon nitride PIC-based multi-color laser engines for life science applications. *Opt. Express* **2021**, *29*, 8635.
(32) Gorin, A.; Jaouad, A.; Grondin, E.; Aimez, V.; Charette, P. Fabrication of silicon nitride waveguides for visible-light using PECVD: a study of the effect of plasma frequency on optical properties. *Opt. Express* **2008**, *16*, 13509−13516.
(33) Bonneville, D. B.; Miller, J. W.; Smyth, C.; Mascher, P.; Bradley, J. D. Low-temperature and low-pressure silicon nitride deposition by ecr-pecvd for optical waveguides. *Appl. Sci. (Switzerland)* **2021**, *11*, 2110.
(34) Museur, L.; Zerr, A.; Kanaev, A. Photoluminescence and electronic transitions in cubic silicon nitride. *Sci. Rep.* **2016**, *6*, 18523.
(35) Steinlechner, J.; Krüger, C.; Martin, I. W.; Bell, A.; Hough, J.; Kaufer, H.; Rowan, S.; Schnabel, R.; Steinlechner, S. Optical absorption of silicon nitride membranes at 1064 nm and at 1550 nm. *Phys. Rev. D* **2017**, *96*, No. 022007.
(36) Stambaugh, C.; Durand, M.; Kemiktarak, U.; Lawall, J. Cavity-enhanced measurements for determining dielectric-membrane thickness and complex index of refraction. *Appl. Opt.* **2014**, *53*, 4930.
(37) Yamada, S.; Schmid, S.; Larsen, T.; Hansen, O.; Boisen, A. Photothermal infrared spectroscopy of airborne samples with mechanical string resonators. *Anal. Chem.* **2013**, *85*, 10531−10535.
(38) Bose, S.; Schmid, S.; Larsen, T.; Keller, S. S.; Sommer-Larsen, P.; Boisen, A.; Almdal, K. Micromechanical string resonators: Analytical tool for thermal characterization of polymers. *ACS Macro Lett.* **2014**, *3*, 55−58.
(39) Andersen, A. J.; Yamada, S.; Pramodkumar, E. K.; Andresen, T. L.; Boisen, A.; Schmid, S. Nanomechanical IR spectroscopy for fast analysis of liquid-dispersed engineered nanomaterials. *Sens. Actuators B Chem.* **2016**, *233*, 667−673.

https://doi.org/10.1021/acs.nanolett.4c02902
Nano Lett. 2024, 24, 11262−11268

(40) Kurek, M.; Carnoy, M.; Larsen, P. E.; Nielsen, L. H.; Hansen, O.; Rades, T.; Schmid, S.; Boisen, A. Nanomechanical Infrared Spectroscopy with Vibrating Filters for Pharmaceutical Analysis. *Angew. Chem., Int. Ed.* **2017**, *56*, 3901−3905.
(41) Luhmann, N.; West, R. G.; Lafleur, J. P.; Schmid, S. Nanoelectromechanical Infrared Spectroscopy with In Situ Separation by Thermal Desorption: NEMS-IR-TD. *ACS Sens.* **2023**, *8*, 1462−1470.
(42) Land, A. T.; Dey Chowdhury, M.; Agrawal, A. R.; Wilson, D. J. Sub-ppm Nanomechanical Absorption Spectroscopy of Silicon Nitride. *Nano Lett.* **2024**, *24*, 7578−7583.
(43) Sementilli, L.; Romero, E.; Bowen, W. P. Nanomechanical Dissipation and Strain Engineering. *Adv. Funct. Mater.* **2022**, *32*, 2105247.
(44) Engelsen, N. J.; Beccari, A.; Kippenberg, T. J. Ultrahigh-quality-factor micro- and nanomechanical resonators using dissipation dilution. *Nat. Nanotechnol.* **2024**, *19*, 725−737.
(45) Guerra, J. A.; Tejada, A.; Töfflinger, J. A.; Grieseler, R.; Korte, L. Band-fluctuations model for the fundamental absorption of crystalline and amorphous semiconductors: A dimensionless joint density of states analysis. *J. Phys. D: Appl. Phys.* **2019**, *52*, 105303.
(46) Sadeghi, P.; Tanzer, M.; Luhmann, N.; Piller, M.; Chien, M. H.; Schmid, S. Thermal Transport and Frequency Response of Localized Modes on Low-Stress Nanomechanical Silicon Nitride Drums Featuring a Phononic-Band-Gap Structure. *Phys. Rev. Appl.* **2020**, *14*, No. 024068.
(47) Schmid, S.; Villanueva, L. G.; Roukes, M. L. *Fundamentals of Nanomechanical Resonators*; Springer International Publishing, 2023.
(48) Klaß, Y. S.; Doster, J.; Bückle, M.; Braive, R.; Weig, E. M. Determining Young's modulus via the eigenmode spectrum of a nanomechanical string resonator. *Appl. Phys. Lett.* **2022**, *121*, No. 083501.
(49) Bergman, T. L.; Lavine, A.; Incropera, F. P. *Fundamentals of heat and mass transfer*; John Wiley, 2017; p 966.
(50) Larsen, T.; Schmid, S.; Grönberg, L.; Niskanen, A. O.; Hassel, J.; Dohn, S.; Boisen, A. Ultrasensitive string-based temperature sensors. *Appl. Phys. Lett.* **2011**, *98*, 121901.
(51) Macleod, H. A. *Thin-Film Optical Filters*; CRC Press, 2010.
(52) Inukai, T. I. T.; Ono, K. O. K. Optical Characteristics of Amorphous Silicon Nitride Thin Films Prepared by Electron Cyclotron Resonance Plasma Chemical Vapor Deposition. *Jpn. J. Appl. Phys.* **1994**, *33*, 2593.
(53) Bulla, D.; Borges, B.; Romero, M.; Morimoto, N.; Neto, L.; Cortes, A. Design and fabrication of SiO/sub 2//Si/sub 3/N/sub 4/ CVD optical waveguides. *1999 SBMO/IEEE MTT-S International Microwave and Optoelectronics Conference*; 1999; pp 454−457, Vol. 2.
(54) Daldosso, N.; Melchiorri, M.; Riboli, F.; Sbrana, F.; Pavesi, L.; Pucker, G.; Kompocholis, C.; Crivellari, M.; Bellutti, P.; Lui, A. Fabrication and optical characterization of thin two-dimensional Si 3N4 waveguides. *Mater. Sci. Semicond. Process.* **2004**, *7*, 453−458.
(55) Sacher, W. D.; Luo, X.; Yang, Y.; Chen, F.-D.; Lordello, T.; Mak, J. C. C.; Liu, X.; Hu, T.; Xue, T.; Guo-Qiang Lo, P.; Roukes, M. L.; Poon, J. K. S. Visible-light silicon nitride waveguide devices and implantable neurophotonic probes on thinned 200 mm silicon wafers. *Opt. Express* **2019**, *27*, 37400.
(56) Worhoff, K.; Klein, E.; Hussein, G.; Driessen, A. Silicon oxynitride based photonics. *2008 10th Anniversary International Conference on Transparent Optical Networks*; 2008; pp 266−269.
(57) Bauer, J. Optical properties, band gap, and surface roughness of Si3N4. *Phys. Status Solidi A* **1977**, *39*, 411−418.
(58) Temple-Boyer, P.; Rossi, C.; Saint-Etienne, E.; Scheid, E. Residual stress in low pressure chemical vapor deposition SiNx films deposited from silane and ammonia. *J. Vac. Sci. Technol. A* **1998**, *16*, 2003−2007.
(59) Garcia, S.; Bravo, D.; Fernandez, M.; Martil, I.; López, F. J. Role of oxygen on the dangling bond configuration of low oxygen content SiNx:H films deposited at room temperature. *Appl. Phys. Lett.* **1995**, *67*, 3263.
(60) Kato, H.; Kashio, N.; Ohki, Y.; Seol, K. S.; Noma, T. Band-tail photoluminescence in hydrogenated amorphous silicon oxynitride and silicon nitride films. *J. Appl. Phys.* **2003**, *93*, 239−244.

https://doi.org/10.1021/acs.nanolett.4c02902
Nano Lett. 2024, 24, 11262−11268